Volume 5, No. 3 March 2026
p-ISSN 2980-4868 | e-ISSN 2980-4841
https://ajesh.ph/index.php/gp

Numerical Study of Gas Flow and Solid Particle Erosion in the Fuel Gas Distribution Octopus Pipe of a Gas Turbine

Rendy Dwi Anggara Prasetia*, Muhammad Agung Bramantya, Joko Waluyo
Universitas Gadjah Mada Yogyakarta, Indonesia
Email: rendydwianggaraprasetia1992@mail.ugm.ac.id*, bramantya@ugm.ac.id, jokowaluyo@ugm.ac.id

ABSTRACT:
The Fuel Gas Distribution Octopus Pipe is a critical component of the Siemens V94.2 gas turbine operated at PLTGU Muara Tawar, responsible for distributing fuel gas to the burners in premix mode. This study aims to analyze the gas-flow characteristics and to predict the erosion rate using a Computational Fluid Dynamics (CFD) approach. Numerical simulations were performed on the 16Mo3 manifold pipe geometry using the Realizable k–ε turbulence model and the Oka erosion prediction model. The operating parameters were varied in terms of gas flow velocity and solid-particle mass flow rate. The results show that the primary erosion mechanism is dominated by inertial impaction, in which particles with a Stokes number greater than 0.1 are unable to follow the gas streamlines in elbow regions and tend to impact the outer elbow wall. Quantitatively, increasing gas velocity significantly raises the maximum erosion rate. At 52.85 m/s, the maximum erosion rate is predicted to be 5.56×10^{-8} kg/m²·s, increasing to 1.83×10^{-7} kg/m²·s at 70.47 m/s (field condition), and reaching 3.30×10^{-7} kg/m²·s at 88.09 m/s. Increasing the solid-particle mass flow rate also increases the erosion rate in an approximately linear manner, from 1.77×10^{-7} kg/m²·s to 2.28×10^{-7} kg/m²·s as the particle mass flow rate increases from 1.31×10^{-7} kg/s to 1.69×10^{-7} kg/s.
Keywords: Fuel Gas Distribution Octopus Pipe; gas turbine; CFD; solid particle erosion; Oka erosion model.

INTRODUCTION

The reliability of electrical energy supply is an important component in supporting sustainable development, as stated in Sustainable Development Goals (SDG) 7 and 9. In facing the transition to a cleaner and more efficient energy system, Gas and Steam Power Plants (PLTGU) have a strategic role because they are able to produce energy with high thermal efficiency and fast response times to load demands.

The Muara Tawar PLTGU is one of the power plants that supplies electricity system needs in Java, Madura, and Bali, with total electricity sales of 1301.24 GWh in September 2024 (Kurniawan, 2024). The Muara Tawar PLTGU consists of blocks 1--2, blocks 3--4, and block 5, with the details of the installed capacity shown in Table 1.1. Currently, the completion of the add-on project in blocks 3--4 is underway for the addition of two units of steam turbines that utilize flue gas from the combustion of gas turbines at a temperature of around 550 °C, thereby increasing the thermal efficiency of the plant (Kehlhofer, 2009).

The Siemens V94.2 gas turbine uses a double-sided chamber silo type, with each chamber having eight burners. The Fuel Gas Distribution Octopus Pipe serves as a critical component of the gas fuel distribution system before the gas enters the burner when the turbine operates in premix mode (Hadzihafizovic, 2025; Madhlopa & Nkhoma, 2025). The Fuel Gas Distribution Octopus Pipe has been in operation since 2004, coinciding with the start of gas turbine operation. This component is classified as critical and must be monitored for reliability and safety. During each inspection, periodic checks are conducted on the elbow areas of the octopus pipe, which are prone to inner-surface wear due to operational conditions. Based on the report on the results of the

assessment of the Fuel Gas Distribution Octopus Pipe during Major Inspection GT 33 of 2023, measurements were conducted at standardized positions to ensure comprehensive, accurate, and reproducible data. The measurements revealed indications of wall thickness thinning, with minimum values of 1.87 mm at position D in BK1 and 1.86 mm at position A in BK2, approaching the minimum wall thickness (MWT) of 1.80 mm.

One of the primary causes of this wall thinning is erosion by solid particles (solid particle erosion) carried in the gas flow. These particles may originate from dust, corrosion scales, sand, or other solid materials entering the supply line or forming within internal system processes (Parsi et al., 2018). The erosion phenomenon significantly impacts the structural integrity of the Fuel Gas Distribution Octopus Pipe. A reduction in pipe thickness approaching the MWT can lead to gas leakage or explosions in the combustor liner, potentially resulting in gas turbine failure. Therefore, a thorough understanding of flow distribution, solid particle motion, and their erosive impact is essential for predictive maintenance planning and system reliability improvement (Strømme, 2015).

Experimental methods for studying this phenomenon are time-consuming, costly, and require specialized equipment. Alternatively, numerical simulations using Computational Fluid Dynamics (CFD) offer an efficient and effective approach to analyzing flow characteristics and interactions with solid particles. Using the CFD approach, pressure distribution, flow velocity, and erosion rate can be mapped in detail, even in physically difficult-to-access areas (Yudhatama et al., 2018).

Several previous studies have demonstrated the capability of CFD to model solid particle erosion. For example, research (Zamani et al., 2017) conducted CFD modeling of erosion in the elbow sections of natural gas pipelines caused by turbulent gas-solid flows. The study concluded that erosion in pipeline elbows is strongly influenced by gas velocity and particle size. Higher flow rates and larger particles result in higher erosion rates. The elbow angle also affects flow patterns and particle distribution, influencing the degree of damage to the inner pipe walls. Another study (Hong et al., 2021) using numerical simulations found that gas velocity, mass flow rate, and sand particle shape coefficient were positively correlated with the maximum erosion rate.

The research gap is particularly significant for the octopus pipe configuration, which features multiple sharp elbows in close succession. In such geometries, secondary flow structures, such as Dean vortices, can develop, potentially concentrating particles into streams (particle roping) and causing non-uniform erosion patterns that intensify downstream (Chen et al., 2004). No previous study has systematically investigated this phenomenon in the specific context of a gas turbine fuel distribution manifold, nor has any study validated CFD predictions against actual field inspection data from an operating power plant over nearly a decade of service.

The urgency of this research is underscored by the safety and economic implications of undetected erosion. Measured wall thickness at some locations is within 0.06 mm of the MWT, indicating that continued operation under current conditions could result in failure within a few years if erosion rates accelerate. A quantitative understanding of erosion mechanisms and accurate

prediction of remaining life are therefore essential for informed decision-making regarding inspection intervals, repair scheduling, and component replacement.

Against this background, this study aims to conduct numerical simulations using CFD on gas flow and solid particle erosion in the fuel gas distribution octopus pipe.

METHOD

Research Object

The research object used in the erosion simulation is the manifold pipe of the fuel gas distribution octopus pipe (Figure 1).

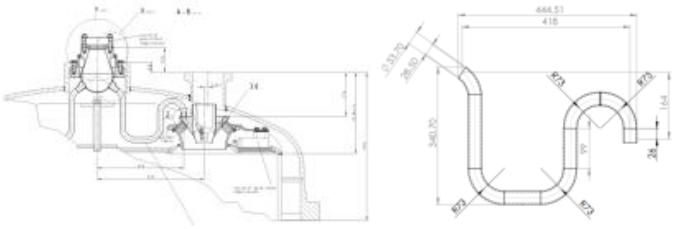

Figure 1. Detail Drawing: (a) Fuel Gas Distribution Octopus Pipe, (b) Manifold Pipe

1. Manifold Pipe Dimension

The manifold pipe used as an erosion simulation object has the dimensions in Table 1. as follows:

Table 1. Manifold Pipe Dimensions [8]

No	Item	Value	Code /Standard of Reference
1	Outer Diameter (mm)	33,70	EN 10220 - Dimensions of pressure steel pipes
2	Inner Diameter (mm)	28,50	EN 10220 - Pipe dimensional tolerance
3	Pipe Thickness (mm)	2,60	EN 10220 - *Nominal wall thickness*
4	Total Length (mm)	617	EN 13480-3 – *Industrial piping design*
5	*Radius Pipe*	73	EN 13480-3 – *Industrial piping design*

Table 1 presents the data on the dimensions of the manifold pipe used in this study along with the reference standards applied. The parameters listed include the outer diameter, inner diameter, pipe thickness, total length, and pipe radius, all of which are expressed in millimeters. The determination of the dimensional value refers to the EN 10220 standard which regulates the dimensions, tolerances, and nominal thickness of steel pipes, as well as the EN 13480-3 standard which is used as a reference in the design of industrial pipes. With this standard reference, the dimensions of the manifold pipe used in the study are expected to meet technical requirements, structural reliability, and conformity to industrial piping design requirements.

2. Fuel Data

Fuel operation parameter data from the performance test report in Table 2. as follows:

Table 2. Gas Data on Manifold Pipe

Parameter	Results	Units
Mass Flow	0,35	kg/s
Pressure	11	Bar
Density	7,83	kg/m3
Viscosite Dynamic	0,0000126	Pa.s
Speed	70,47	m/s

Table 2 presents the parameter data of the gas flowing in the manifold pipe which is used as an input to the operating conditions in this study. The parameters displayed include mass flow rate, pressure, density, dynamic viscosity, and gas flow velocity and its units. This data is used to represent the fluid characteristics and actual flow conditions within the pipeline, which further serves as the basis for the analysis of flow behavior, fluid force calculation, as well as the evaluation of the influence of gas flow on the performance and degradation of the pipe manifold.

3. Solid Particle Data

Solid particle data such as diameter size and particle count are taken using several assumptions, namely:

Table 3. Solid Particle Data

Parameter	Results	Units
Density	2800	kg/m3
Mass Flow Rate	0,000000135	kg/s
Diameter	2	µm

Parameter Variation Simulation

In this study, the parameters of gas flow velocity and solid particle rate were varied to evaluate their effect on the magnitude of the erosion produced. The variation of the parameters to be carried out is shown in Table 4.

Table 4. Variation in Gas Velocity and Mass Flow Parameters of Solid Particles

Variation	Gas Velocity Variation (m/s)	*Mass Flow* Gas (kg/s)	*Mass Flow* Particle (kg/s)	Remarks
A	52,85	0,2643	1,35 ×10⁻7	*Low Gas Velocity*
B	70,47	0,3525	1,35 ×10⁻7	Operating Conditions
C	88,09	0,4406	1,35 ×10⁻7	*High Gas Velocity*
D	70,47	0,3525	1,01×10⁻7	*Low Particle Loading*
E	70,47	0,3525	1,50×10⁻7	*Moderate Particle Loading*
F	70,47	0,3525	1,69×10⁻7	*High Particle Loading*

Geometry and Fluid Domain Creation

The model made is in the form of a manifold *pipe fuel gas distribution octopus pipe* geometry (Figure 2). The *drawing* process using *Solidwork* 2021 software is based on the design drawings in the *Siemens V94.2 Gas Turbine manual* book (Figure 1).

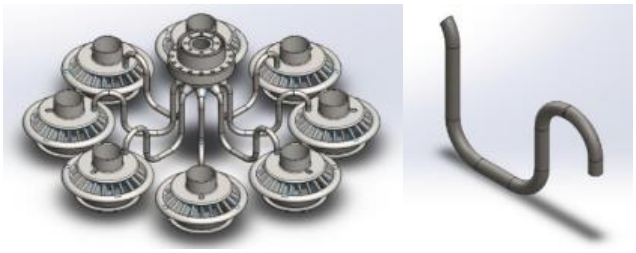

Gambar 2. *Geometri Manifold Pipe: (a) Fuel Gas Distribution Octopus Pipe, (b) Manifold Pipe*

In CFDs, one of the most important things to pay attention to is the creation of a fluid domain from the simulation. The fluid domain of the numerical simulation will affect the results that the simulation outputs. The creation of fluid domains is shown in Figure 3 which consists of:

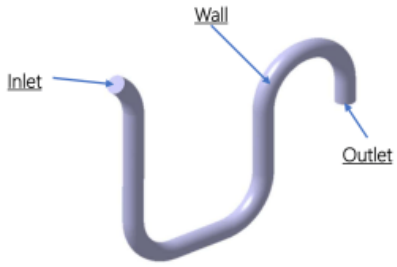

Figure 3. Fluid Domain

Furthermore, to obtain a structured mesh it is necessary to divide the fluid domain into several parts as shown in Figure 4. The pipe cross-section is divided into five areas, formed from a square with the same center as the circle and the nearest line connecting the square corner with the circle (Atmaja et al., 2020).

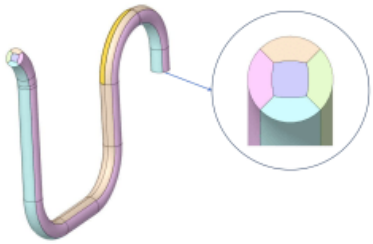

Figure 4. Fluid Domain Divisions

Meshing dan *Grid Independent Test*

The fluid domain has many elbows, so multizone type mesh with a hexa shape was chosen because of its advantages for meshes with complex models, faster computation and more efficient use of elements (Alhassan & Bashiru, 2021). The mesh is compacted near the manifold pipe wall and elbow area, and inflation is added to capture the velocity gradient and improve the accuracy of particle trajectory prediction and erosion. The results of the meshing are presented in Table 5.

Table 5. *Meshing Results*

	Element	*Mesh* Global	Detail *near-wall*
M 1	257.508	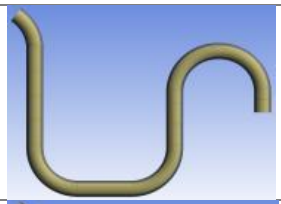	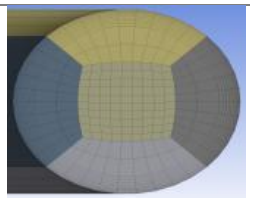
M 2	845.152		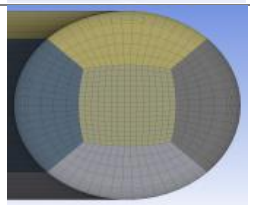
M 3	1.277.100	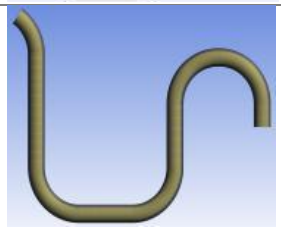	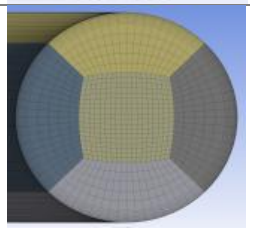
M 4	1.648.640	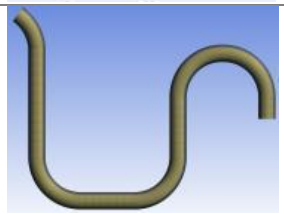	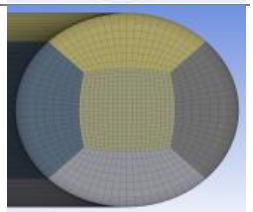
M 5	2.112.880	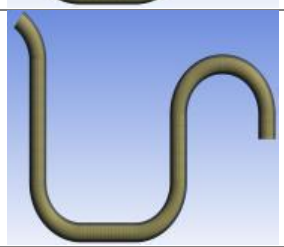	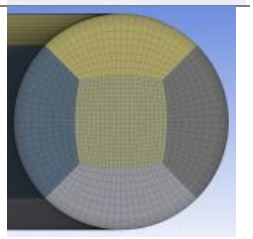

Table 6. Mesh *Quality Results*

		M1	M2	M3	M4	M5
Elements		257.508	845.152	1.277.100	1.648.640	2.112.880
Skewness	Min	$1{,}13 \times 10^{-3}$	$3{,}64 \times 10^{-3}$	$2{,}01 \times 10^{-3}$	$1{,}91 \times 10^{-3}$	$1{,}77 \times 10^{-3}$
	Max	0,37	0,37	0,37	0,37	0,37
	Avg	0,09	0,07	0,07	0,07	0,07
Ortho	Min	0,27	0,88	0,87	0,87	0,87

	M1	M2	M3	M4	M5
Max	0,99	1	1	1	1
Avg	0,98	0,99	0,99	0,99	0,99

The mesh quality results data are then compared with the mesh quality range. The results of the comparison showed that the skewness category of the four simulated meshing models was included in the quality of verry good. In the orthogonal quality category of the four simulated meshing models, only M1 is included in good quality, while M2, M3, M4 and M5 are included in very good quality. This shows that the mesh quality model 3D fluid domain of the four meshing models for simulation is good and can be continued in the next process.

Table 7. *Grid Independent Test Area-Weighted Average DPM Erosion Rate (Oka)* Results in *patches* A, B, C, D, E

	Element	***Erosion* (kg/m²·s)**	***Thinning* (mm/yr)**	**Δ% vs previous *mesh***
M1	257.508	9,85E-09	0,039	-
M2	845.152	8,76E-09	0,035	11,09%
M3	1.277.100	7,70E-09	0,031	12,08%
M4	1.648.640	7,54E-09	0,030	2,03%
M5	2.112.880	7,18E-09	0,029	4,87%

From Table 7, between M1 and M2 there was a change in simulation results of 11.09%. Furthermore, between M2 and M3, the change in simulation results was 12.08%. Furthermore, between M3 and M4, the change in simulation results was only 2.03%. between M4 and M5, the change in simulation results increased again by 4.87%. M3 with several elements of 1,277,100 can be used as a model for the first simulation with Variation B with a gas velocity of 70.47 m/s, a gas mass of 0.3525 kg/s and a particle mass of 1.35 x 10-7 kg/s according to operating conditions (Table 4).

Validation of Simulation Results

From the results of the measurement of the wall thickness of the manifold pipe, a minimum value was taken for each patch A, B, C, D, E. With the equivalent operating hour (EOH) of GT 3.3, which is 86,490 hours (9.86 years), a thinning rate was calculated, the results of which are shown in Table 8. In order to validate with the results of the CFD simulation, it is necessary to convert units in kg/m2s using the following Equation 1:

$$E = \dot{t}(mm/yr)x\left(\frac{1x10^{-3}m/mm}{31560000\ s/yr}\right)x\rho_t \qquad (1)$$

Tabel 8. Data Thinning Rate Manifold Pipe

Patch	**t_o (mm)**	**t_*min* (mm)**	**Δt (mm)**	***Thinning rate* (mm/yr)**	***E (kg/m2·s)***
A	2,60	1,86	0,74	0,075	1,88 ×10⁻8
B	2,60	1,89	0,71	0,072	1,80 ×10⁻8

Patch	t_0 (mm)	t_*min* (mm)	Δt (mm)	*Thinning rate* (mm/yr)	*E (kg/m2·s)*
C	2,60	2,13	0,47	0,048	1,19 ×10⁻8
D	2,60	1,87	0,73	0,074	1,85 ×10⁻8
E	2,60	1,88	0,72	0,073	1,83 ×10⁻8
AVG	2,60	1,926	0,674	0,068	1,71 ×10⁻8

Table 8 presents the results of the thinning rate calculation on the manifold pipe based on the measurement of pipe thickness at several observation points (patch A–E). The data displayed included initial pipe thickness (t_0), minimum measured thickness (t_min), thickness difference (Δt), thinning rate in mm/year, and mass loss rate (E) in kg/m²·s. The thinning rate value indicates the degree of degradation of the pipe material due to the depletion mechanism during the operating period, while the E value represents the amount of material loss per unit area and time. The average (AVG) of all patches is used to describe the general condition of the manifold pipe, so this table serves as the basis for evaluating the material degradation rate and estimating the service life of the pipe in this study.

RESULTS AND DISCUSSION

Reynolds Number

The Reynolds Number states the ratio between the inertial force and the viscosity in a fluid. *The Reynolds Number* is expressed in Equation 1:

$$Re = \frac{\rho U D}{\mu} \qquad (2)$$

With a reynolds number value of 1.24x106, it can be stated that the gas flow in the *manifold pipe* is a full turbulent flow.

Stokes Number

The Stokes Number (Stk) is a number without units that indicates how much the inertia of a particle is compared to the ability of a fluid to direct it along the flow. The Stokes Number measures the "stiffness" of a particle to changes in the direction of gas flow. If the particles are so light that they are easily carried away by the flow (small Stk). If the particles are heavy/large so that it is difficult to turn and cause frequent collisions with the wall (large Stk). Equation 2 to calculate the Stokes Number:

$$Stk = \frac{\rho_p d_p^2 U}{18 \mu D} \qquad (3)$$

Solid Loading Ratio (SLR*)*

The Solid Loading Ratio (SLR) is the ratio of the mass of solid particles to the mass of flowing gaseous fluids. SLR can be calculated using Equation 3.

$$r_s = \frac{\dot{m}_p}{\dot{m}_g} \qquad (4)$$

The smaller the loading ratio, the fewer particles are compared to gases. The phase is very dilute, the mass that punches the wall is very small. Because it has an SLR value of 3.82 x 10-7. The result includes an SLR range of less than 10-4, hence the use of one-way coupling (particles do not change the flow).

Validation of Simulation Results

The simulation erosion rate data was extracted at the locations of the pipe wall that were equivalent to patches A, B, C, D, E during the measurement of the thickness of the pipe in the field. The extraction area (Figure 6), adjusted to the dimensions of the ultrasonic probe used in the inspection, thus allowing for a direct comparison between the simulation results and the field data.

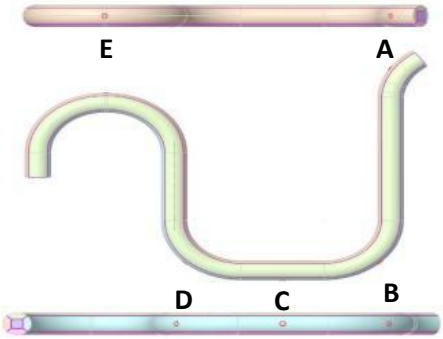

Figure 6. Location of Erosion Data Extraction Patch

The value of the erosion rate from the simulation of variation B with a gas velocity of 70.47 m/s, a gas mass of 0.3525 kg/s and a particle mass flow of 1.35 x $^{10-7}$ kg/s according to field conditions, compared to the estimated rate of pipe wall thinning based on field thickness measurement data.

Table 9. Comparison of Field Erosion vs Simulation Erosion

Patch	E_Field (kg/m²·s)	E_CFD (kg/m²·s)	CFD/Field Ratio	Relative Error (%)
A	1,88 x 10^{-8}	2,04 x 10^{-8}	1,09	8,51
B	1,80 x 10^{-8}	1,75 x 10^{-8}	0,97	-2,78
C	1,19 x 10^{-8}	1,16 x 10^{-8}	0,98	-2,52
D	1,85 x 10^{-8}	1,81 x 10^{-8}	0,98	-2,16
E	1,83 x 10^{-8}	1,73 x 10^{-8}	0,95	-5,46

Methods and Solutions in Numerical Solving

Table 10. Numerical Solution Method

Category	Parameter	Method/Scheme
Pressure–Velocity Coupling	Clutch Scheme	SIMPLE
Typical Flow	Momentum Flux	Rhie–Chow momentum based (Auto Select)
Spatial Discretization	Gradient	Least Squares Cell Based
Spatial Discretization	Pressure	Second Order
Spatial Discretization	Momentum	Second Order Upwind
Spatial Discretization	Turbulent Kinetic Energy (k)	Second Order Upwind
Spatial Discretization	Turbulent Dissipation Rate (ε)	Second Order Upwind
Time Discretization	Pseudo Time Method	Off

Table 10 describes the arrangement of the numerical solution method and scheme used in the Computational Fluid Dynamics (CFD) simulation in this study. The parameters displayed include pressure–speed coupling methods, momentum flux calculation schemes, and spatial discretization schemes for mainflow and turbulence variables, all of which aim to improve the accuracy and stability of numerical solutions. The use of the SIMPLE scheme and second-order discretization shows that the simulation is carried out with a numerical approach that can represent the flow behavior more accurately, so that the simulation results obtained can be used as a basis for reliable analysis of fluid flow in the manifold pipe.

The realizable turbulence model k–ε was chosen because it has better performance in predicting flows with high-velocity gradients, secondary flows, and curvature effects, which are common in pipe elbows. This model is widely used in numerical studies of erosion in gas pipelines because it can adequately represent the average flow field that affects the trajectory and impact velocity of particles with efficient computational costs.

Characteristics of Gas Flow in Pipelines

Gas Flow Speed Distribution

From the simulation of variation A (gas velocity 52.85 m/s, gas mass flow 0.2643 kg/s and particle mass flow 1.35 x 10-7 kg/s), variation B (gas velocity 70.47 m/s, gas mass flow 0.3525 kg/s and particle mass flow 1.35 x 10-7 kg/s) and variation C (gas velocity 88.09 m/s, gas mass flow 0.4406 kg/s and particle mass flow 1.35 x 10-7 kg/s) are obtained the gas flow speed distribution in Figure 7.

A

B

C

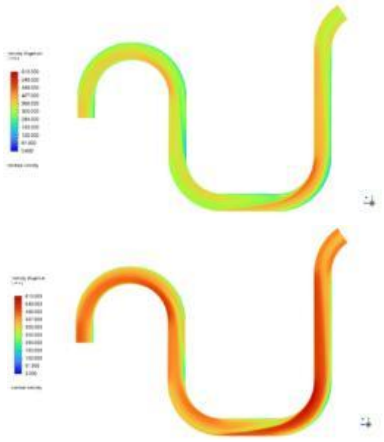

Figure 7. Gas Flow Velocity Distribution, a) variation A, b) variation B, and c) variation C

An in-depth comparative analysis of these three results reveals two key findings. First, qualitatively, the flow field topology shows consistency across the simulated speed range. In all three cases, the dominant flow phenomenon is the formation of a jet effect, where the flow experiences a significant acceleration along the inner wall of the bend. The jet effect is a well-documented characteristic in the literature for flows in geometry with sharp discontinuities. In contrast to long-radius bends where centrifugal forces dominate, in sharp bends or mitre bends, there is a massive flow separation on the outer wall [12]. This forces the fluid to take the shortest path along the inner wall, where it accelerates to form a high-speed jet, a phenomenon that was also observed in flow analysis at T-junctions [15]. Nonetheless, the DPM erosion literature consistently confirms that the erosion location of solid particles is not determined by the location of the maximum gas velocity, but rather by the particle inertia represented by the Stokes number [15]. Therefore, the results of this simulation, which show a jet of gas on the inner side but maximum erosion on the outer side, are physically consistent and supported by the fundamental theory of phase trajectory decoupling in a two-phase flow.

Pressure, Velocity Vector and Gas Flow Line

Figure 8. Gas Flow Pressure Distribution at Variation B

Figure 8 of the static pressure contours for variation B (gas velocity 70.47 m/s), shows the high pressure stagnation zone on the outer wall and the low pressure zone on the inner wall. The response of fluid flow to this pressure gradient is visualized in detail through the plot of velocity vectors (Figure 9) and flow lines (Figure 10). The flow line clearly shows how the fluid is sucked into the low-pressure zone, where the trajectory contracts and accelerates forming a jet effect. In

contrast, in the high-pressure stagnation zone, the main flow experiences massive flow separation, a characteristic of flow in sharp bends and mitre bends as discussed by (Parsi, 2015). The vector plot (Figure 9) confirms this separation zone by showing a very low-energy area near the outer wall.

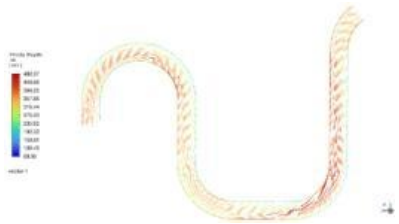

Figure 9. *Velocity Vector of* Gas Flow Magnitude at Variation B

Figure 10. *Pathlines Velocity Gas Flow Magnitude* on Variation B

Figure 8 of the velocity vector plot, showing the accelerated flow on the inner wall and the low-energy chaotic flow zone on the outer wall. Figure 9 Visualization of the Flow Line (pathlines), confirming the formation of the core jet and flow separation zone.

The integrated analysis of Figures 6, 7 and 8 provides a complete mechanistic explanation of why maximum erosion occurs in the outer wall, which is very much in line with the theory of trajectory separation from (Bellman & Levy, 1981). Solid particles with transition inertia (Stk = 0.1221) fail to follow the sharp turn of the gas jet effect. Its straighter trajectory takes it across a low-energy separation zone near the outer wall. Because the velocity of the fluid within this separation zone is very low, the drag force of the fluid against the particles is minimal. This is a crucial point, as the particle can retain most of its momentum before hitting the outer wall, a mechanism consistent with the findings (Boyce, 2012) suggesting that the efficiency of the collision is highly dependent on the Stokes number.

Solid Particle Path Pattern

The visualization of the trajectory colored by particle diameter, presented in Figure 12, serves as a crucial methodological validation. The uniform color across the particle's trajectory confirms that the simulation consistently uses mono-disperse particles with a single diameter, i.e. 2 μm. This validation is critical because it ensures that any variation in the particle's trajectory or velocity is caused purely by hydrodynamic interactions with the fluid, not by differences in the intrinsic properties of the particles. In addition, it confirms the validity of the application of the Oka erosion model, whose parameters are highly sensitive to the diameter of the fisting particles.

Figure 12. Particles Track Diameter on Variation B

Next, Figure 13 presents a visualization of the colored trajectory based on the magnitude of the particle velocity. This image directly visualizes the transfer of kinetic energy from the gas phase to the solid phase. The particles undergo significant acceleration as they enter the jet effect along the inner wall, which is characterized by a change in the color of the trajectory to red (high velocity). The most significant finding is that the particles maintain this high velocity as their trajectory deviates from the gas flow and crosses the pipeline's cross-section towards the outer wall. This phenomenon visually demonstrates the principle of conservation of particle momentum due to inertia. Although the particles cross the low-velocity fluid zone near the outer wall (as shown in the previous vector analysis), their inertia (Stk = 0.1221) prevents them from slowing down significantly. This high impact velocity, which is maintained by the particles until the last moment before impact, is the most critical input variable in the erosion model, where the rate of erosion often has a power-law relationship with the velocity of the collision ($E \propto Vn$ with $n > 2$), explaining why the erosion that occurs is so severe.

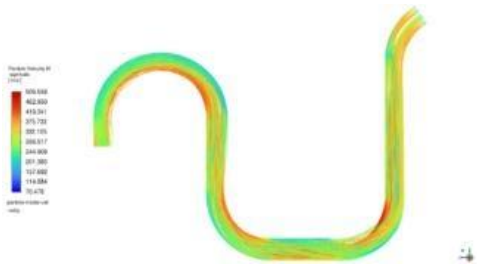

Figure 13. Particles Track Velocity Magnitude on Variation B

Finally, Figure 14 shows a trajectory colored based on the particle's residence time, providing a temporal picture of the particles causing the erosion. This visualization shows a smooth, progressive color gradient along the main trajectory of the particles that are pounding the wall. This indicates that the dominant erosion mechanism is caused by a continuous flow of particles with a relatively narrow residence time distribution (RTD). No particles are observed to be trapped in the recirculation zone for a long time (which will be marked by a locally bright red color). This implies that the erosion that occurs is the result of a stable and predictable direct impact, rather than of more complex processes such as particle accumulation or periodic particle removal from the vortex zone. These findings simplify the interpretation of erosion mechanisms into a stable and continuous inertial collision process.

Figure 14. Particles Residence Time on Variation B

Collectively, these three visualizations paint a complete picture, where particles of uniform diameter (Figure 11) are accelerated to high speeds by gas jets (Figure 12) and due to their inertia, travel a relatively direct and rapid collision trajectory (Figure 13) towards the outer wall, resulting in a predictable erosion mechanism that is highly dependent on the momentum retained by the particles.

Distribution of Erosion Rate in Manifold Pipe

The erosion rate distribution obtained from the simulation showed a non-uniform pattern along the pipe wall. The erosion value is relatively small in the straight segment of the pipe and significantly increases in the elbow area. The peak of the erosion rate is localized on the outer side of the turn, which corresponds directly to the impact location of the particle with high velocity and impact angle. These results are consistent with Oka's erosion model, which states that the erosion rate increases sharply with an increase in impact velocity and is significantly influenced by the angle of impact (Oka et al., 2005).

Table 11. Erosion Contour Results (operating conditions, gas velocity 70.47 m/s, gas mass flow 0.3525 kg/s and particle mass flow 1.35 x 10-7 kg/s)

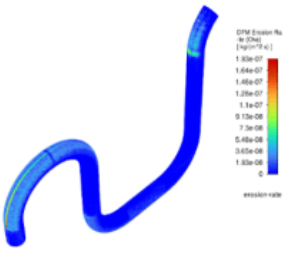	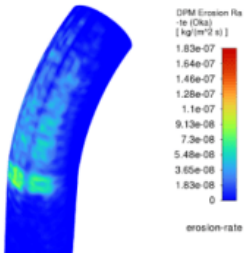	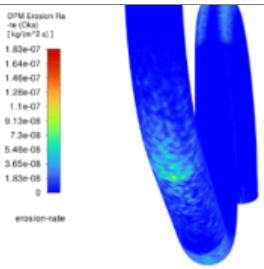
Isometric	*Patch* A	*Patch* B
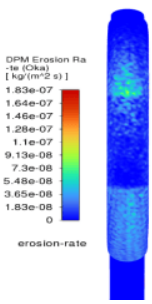	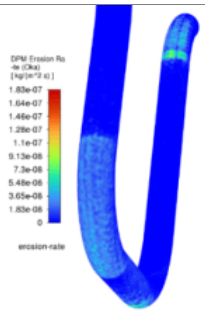	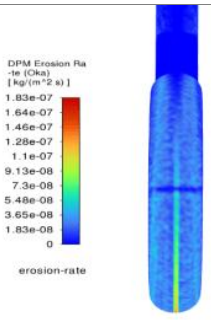
Patch C	*Patch* D	*Patch* E

CFD simulations show that the rate of erosion of the pipeline walls increases significantly as the speed of the gas flow increases. When compared to the results of field inspections, the average actual thinning is 0.068 mm/year. This value is between the CFD predicted values, which are 0.06–0.08 mm/year. Thus, the CFD model can adequately represent the actual erosion phenomenon. However, the maximum erosion value of CFDs is higher than the field average. This can be explained because CFD calculates local hotspot erosion, while field measurements use a probe thickness with a larger measurement area.

Based on an initial thickness of 2.6 mm and a current thickness of ±1.9 mm, an operating life of about 9–10 years is obtained. CFD results estimate the remaining lifespan between 2 and 80 years depending on the variation of operations and location. The most practically relevant values are on critical patches and variations of operations that represent actual conditions. For these conditions, the estimated remaining life is in the range of 3-5 years, which is still consistent with the normal preventive inspection schedule.

Critical Location of Erosion Rate on Manifold Pipe

Mapping and quantification of erosion rates across the entire internal surface of the pipeline, allowing the identification of the locations most vulnerable to material failure. Figure 15 and Figure 16 present a visualization of the erosion rate contour for the simulation of variation B (field conditions, gas velocity 70.47 m/s, gas mass flow 0.3525 kg/s and particle mass flow 1.35 x 10-7 kg/s) from isometric views and views focused on the maximum erosion point.

Figure 15. Contour of maximum erosion rate on manifold pipe

Consistently, the highest erosion rate is present on the outer wall surface of each sharp bend, which validates the inertial impact mechanism. The most critical erosion, where the intensity of erosion escalates or amplifies progressively along the downstream, reaching its peak at the last bend before the outlet.

Max Erosion Rate VS Gas Velocity Analysis

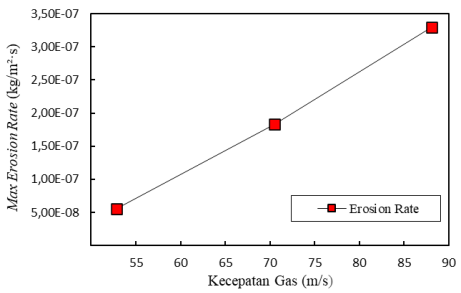

Figure 17. Gas Velocity Graph Against Erosion Rate

The relationship between gas velocity and erosion rate shows a strong trend of constant increase. In general, an increase in gas velocity results in a significant increase in erosion rate. Main trend in variation A with a gas velocity of 52.85 m/s, the erosion rate is still low, which is 5.56×10^{-8} kg/m²·s. When the velocity rises to 70.47 m/s, which is variation B (operating condition), the erosion rate increases drastically to the range of 1.83×10^{-7} kg/m²·s. At variation C with a gas velocity of 88.09 m/s, erosion reaches a maximum value of 3.30×10^{-7} kg/m²·s. This is consistent with the erosion of the Oka model, where the power-law relationship is $E \propto V^n$, with exponents n ≈ 2–3. This means that a slight increase in speed can create a spike in erosion rate. The physical cause of the increase in velocity results in an increase in the kinetic energy of the particle where $E_k = \frac{1}{2}mV^2$. So that the same particles will hit the wall harder, cause greater plastic deformation, and trigger more aggressive micro-cutting and micro-fracture. Higher speeds cause particles to hit surfaces more often in the same time.

Max *Erosion Rate VS Mass Flow* Analysis of Solid Particles

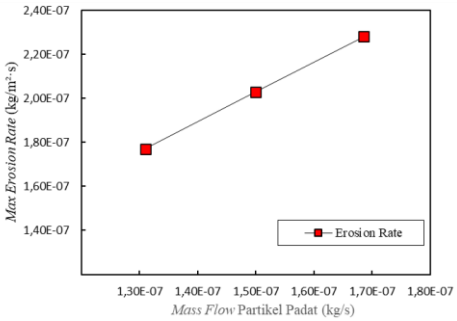

Figure 18. Solid Particle Mass Flow Graph Against Erosion Rate

In the initial condition, when the particle mass flow was 1.31×10^{-7} kg/s, the predicted erosion rate was 1.77×10^{-7} kg/m²·s. This value increased to 2.03×10^{-7} kg/m²·s when the particle mass flow was increased to 1.50×10^{-7} kg/s, and continued to increase to 2.28×10^{-7} kg/m²·s at the highest mass flow, which was 1.69×10^{-7} kg/s.

Physically, this phenomenon is consistent with the mechanism of solid particle erosion, where the amount of material loss is greatly influenced by the number of particles that hit the wall per unit of time. As long as the gas flow speed and impact angle are relatively constant, the kinetic energy per particle does not undergo significant changes, so the increase in erosion is completely dominated by the increase in the number of particles carrying impact energy to the wall surface. Thus, the results of this simulation show that particle loading is the dominant parameter of the erosion rate, while the influence of other parameters such as fluid or thermal velocity is relatively small in this study.

Remaining Life VS Gas Velocity Analysis

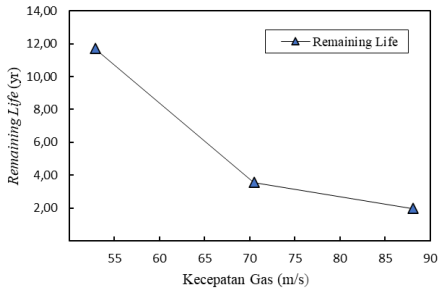

Figure 19. Gas Velocity Graph Against Remaining Life

Figure 19 shows a graph of the inverse relationship between the velocity of the gas in the pipeline and the remaining life (the remaining life of the pipe due to erosion). In general, the higher the gas flow speed, the greater the impact force of the particles against the pipe wall, so that the erosion rate increases and the remaining life of the pipe decreases. The main trend at the lowest speed of 52.85 m/s, variation A, the remaining life of the pipe reaches 11.7 years, is the highest value. At a top speed of 88.09 m/s, the C variation, the remaining lifespan drops drastically to 2 years, which is the lowest value.

Analysis of Remaining Life VS Mass Flow of Solid Particles

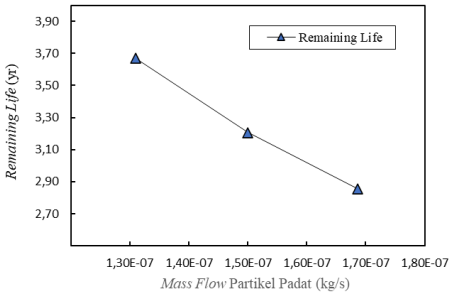

Figure 20. Solid Particle Mass Flow Graph Against Remaining Life

The remaining life graph shows a consistent downward trend towards an increase in the mass flow of solid particles (Figure 20). At the lowest solid particle mass flow condition (1.31×10^{-7} kg/s), the predicted remaining life is 3.67 years. When the mass flow of solid particles increased to 1.50×10^{-7} kg/s, the remaining life decreased to 3.21 years, and continued to decrease to 2.85 years at the highest solid particle mass flow condition of 1.69×10^{-7} kg/s. Thus, an increase in particle mass flow by 29% led to a decrease in remaining life by 22%.

CONCLUSION

The primary erosion mechanism in the fuel gas distribution octopus pipe is inertial impaction, where solid particles with significant inertia ($Stk > 0.1$) fail to follow the sharp curvature of the gas flow and impact the outer wall of elbows, resulting in maximum erosion at locations distinct from the peak gas velocity. Erosion is non-uniform and amplifies downstream

due to the formation and interaction of secondary flows, such as Dean vortices, which trigger particle roping. The erosion rate is highly sensitive and exhibits a nonlinear, exponential dependence on gas velocity, with the final elbow before the outlet consistently experiencing the highest erosion and identified as the most critical failure point. Since these findings are based on numerical simulations with one-way coupling and the Oka erosion model, future research should focus on experimental validation using test rigs and techniques like Electrical Resistance probes or profilometry, while also exploring two-way or four-way coupling to account for momentum feedback and inter-particle collisions. Additionally, studies incorporating poly-disperse particle size distributions and alternative erosion models (e.g., DNV, E/CRC Tulsa) are recommended to improve the accuracy and confidence of erosion predictions under realistic field conditions.

REFERENCES

Alhassan, M., & Bashiru, Y. (2021). Carbon equivalent fundamentals in evaluating the weldability of microalloy and low alloy steels. *World Journal of Engineering and Technology*, *9*(5), 838–853. https://doi.org/10.4236/wjet.2021.95059

Atmaja, H. J., Kamal, S., & Sugiyono, S. (2020). Simulasi numerik prediksi erosi aliran fasa cair-gas berpasir pada belokan pipa sumur minyak mentah menggunakan model Finnie, McLaury dan Oka. *Journal of Mechanical Design and Testing*, *2*(1), 47. https://doi.org/10.22146/jmdt.53724

Bellman, R., & Levy, A. (1981). Erosion mechanism in ductile metals. *Wear*, *70*, 1–28.

Boyce, M. P. (2012). Combustors. In *Gas turbine engineering handbook* (pp. 355–407). Elsevier. https://doi.org/10.1016/b978-0-12-383842-1.00010-x

Chen, X., McLaury, B. S., & Shirazi, S. A. (2004). Application and experimental validation of a computational fluid dynamics (CFD)-based erosion prediction model in elbows and plugged tees. *Computers and Fluids*, *33*(10), 1251–1272. https://doi.org/10.1016/j.compfluid.2004.02.003

Hadzihafizovic, D. (2025). Combustion of LPG Burners and Ancillary Equipment Bulk Distribution and Handling LPG. *Available at SSRN 5845342*.

Hong, B., Li, Y., Li, X., Ji, S., Yu, Y., Fan, D., Qian, Y., Guo, J., & Gong, J. (2021). Numerical simulation of gas-solid two-phase erosion for elbow and tee pipe in gas field. *Energies*, *14*(20), 6609. https://doi.org/10.3390/en14206609

Kehlhofer, R. (2009). *Combined-cycle gas and steam turbine power plant* (3rd ed.). PennWell.

Kurniawan, A. (2024). *Laporan kontrak kinerja unit pembangkitan Muara Tawar*.

Madhlopa, A., & Nkhoma, R. (2025). Gas turbine fuels and fuel systems. In *Principles of Solar Gas Turbines for Generating Electricity* (pp. 45–70). Springer.

Oka, Y. I., Okamura, K., & Yoshida, T. (2005). Practical estimation of erosion damage caused by solid particle impact: Part 1: Effects of impact parameters on a predictive equation. *Wear*, *259*(1–6), 95–101. https://doi.org/10.1016/j.wear.2005.01.039

Parsi, M. (2015). *Sand particle erosion in vertical slug/churn flow* [Doctoral dissertation, The University of Tulsa].

Parsi, M., Arabnejad, H., Al-Sarkhi, A., Zahedi, P., Vleira, R. E., Sharma, P., & McLaury, B. S. (2018). A new correlation for predicting solid particle erosion caused by gas-sand flow in elbows. *Proceedings of the Annual Offshore Technology Conference*, *4*, 2725–2742. https://doi.org/10.4043/28995-ms

Siemens. (2015). *Basic operation training SGT-2000E*.

Strømme, E. G. (2015). *Simulation and evaluation of slurry erosion* [Master's thesis, Norwegian University of Science and Technology]. https://brage.bibsys.no/xmlui/handle/11250/2350092

Yudhatama, I. W., Purbawanto, M. I., & Jatimurti, W. (2018). Computational fluid dynamics (CFD) simulation of sand particle erosion in turbulent gas fluid flow in vertical-horizontal elbow. *Jurnal Teknik ITS*, *7*(2), 1–6. https://doi.org/10.12962/j23373539.v7i2.30445

Zamani, M., Seddighi, S., & Nazif, H. R. (2017). Erosion of natural gas elbows due to rotating particles in turbulent gas-solid flow. *Journal of Natural Gas Science and Engineering*, *40*, 91–113. https://doi.org/10.1016/j.jngse.2017.01.034